Constraints on grain size and stable iron phases in the uppermost Inner Core from multiple scattering modeling of seismic velocity and attenuation

Marie Calvet, Ludovic Margerin

Constraints on grain size and stable iron phases in the uppermost Inner Core from multiple scattering modeling of seismic velocity and attenuation

Marie Calvet [a,b,*] Ludovic Margerin [c]

[a]Laboratoire de Géophysique Interne et Tectonophysique, BP 53, 38041 Grenoble cedex 9, FRANCE

[b]Now at Laboratoire de Dynamique Terrestre et Planétaire, Observatoire Midi-Pyrénées, 14 avenue Edouard Belin, 31400 Toulouse, FRANCE

[c]Centre Européen de Recherche et d'Enseignement des Géosciences de l'Environnement, BP 80, 13545 Aix-en-Provence, FRANCE

Abstract

We propose to model the uppermost inner core as an aggregate of randomly oriented anisotropic "patches". A patch is defined as an assemblage of a possibly large number of crystals with identically oriented crystallographic axes. This simple model accounts for the observed velocity isotropy of short period body waves, and offers a reasonable physical interpretation for the scatterers detected at the top of the inner core. From rigorous multiple scattering modeling of seismic wave propagation through the aggregate, we obtain strong constraints on both the size and the elastic constants of iron patches. In a first step, we study the phase velocity and scattering attenuation of aggregates composed of hexagonal and cubic crys-

tals, whose elastic constants have been published in the mineral physics literature. The predicted attenuations for P waves vary over two orders of magnitude. Our calculations demonstrate that scattering attenuation is extremely sensitive to the anisotropic properties of single crystals and offers an attractive way to discriminate among iron models with e.g. identical Voigt average speeds. When anisotropy of elastic constants is pronounced, we find that the S wavespeed in the aggregate can be as much as 15% lower than the Voigt average shear velocity of a single crystal. In a second step, we perform a systematic search for iron models compatible with measured seismic velocities and attenuations. An iron model is characterized by its symmetry (cubic or hexagonal), elastic constants, and patch size. Independent of the crystal symmetry, we infer a most likely size of patch of the order of 400 m. Recent *bcc* iron models from the literature are in very good agreement with the most probable elastic constants of cubic crystals found in our inversion. Our study (1) suggests that the presence of melt may not be required to explain the low shear wavespeeds in the inner core and (2) supports the recent experimental results on the stability of cubic iron in the inner core, at least in its upper part.

Key words: multiple scattering, attenuation, dispersion, iron elastic properties, grain size, Earth's inner core

1 Introduction

The gross seismic features of the inner core are nowadays known with some confidence. The uppermost inner core, where crystallization of iron occurs, is a peculiar region with isotropic seismic velocities, strong attenuation and

* Corresponding author
Email addresses: calvet@dtp.obs-mip.fr (Marie Calvet),
margerin@cerege.fr (Ludovic Margerin).

where the presence of scatterers has been detected. Mineral physicists have concentrated a lot of efforts on experimental and theoretical investigations of elastic properties of iron at inner core condition. In spite of remarkable advances, fundamental questions pertaining to the symmetry class and the anisotropy parameters of iron are still actively debated and no clear consensus has emerged yet. In this study, we use the velocity and attenuation properties of seismic waves inferred from previous studies to propose a simple physical model of the uppermost inner core. Using a rigorous multiple scattering approach based on the Dyson equation for elastic waves in random media, we analyze critically various iron models from the mineral physics literature and give constraints on the possible stable iron phases in the inner core. In what follows, the necessary seismological and mineralogical data are reviewed and our approach is described.

1.1 Seismic observations and mineral physics

Traveltime analyses of seismic body waves have revealed that the Earth's inner core is anisotropic with about 1-3% velocity anisotropy and a fast direction of propagation parallel to Earth's rotation axis. Depth variations have been observed with an isotropic layer overlying deep anisotropy (Shearer, 1994; Su and Dziewonski, 1995; Creager, 1999; Garcia and Souriau, 2000; Wen and F. Niu, 2002) and a change of velocity anisotropy near the centre of the inner core (Ishii and Dziewonski, 2002; Beghein and Trampert, 2003; Calvet et al., 2006). The inner core is heterogeneous at different scales with hemispherical velocity variations (Niu and Wen, 2001; Garcia, 2002; Cao and Romanowicz, 2004), continent scale (Stroujkova and Cormier, 2004) and

short wavelength features (20-200 km) (Bréger et al., 1999). There are strong evidences for the concentration of very small scale heterogeneities at the top of the inner core. The *PKIKP* wave that bottoms in the uppermost inner core is strongly attenuated compared to outer core phases. In addition, its frequency spectrum is depleted in high frequencies. Various studies proposed a range of values for *P*-wave quality factor between 100 and 400 in the uppermost 200 km with possible lateral variations (e.g. Souriau and Roudil, 1995; Wen and F. Niu, 2002; Cao and Romanowicz, 2004; Yu and Wen, 2006). Viscoelastic and scattering attenuation are candidates to explain this observation (Li and Cormier, 2002; Cormier and Li, 2002) but the latter mechanism seems more consistent with the strong coda of the reflected *P* wave generated at the inner core boundary (Vidale and Earle, 2000; Poupinet and Kennett, 2004; Koper et al., 2004; Krasnoshchekov et al., 2005; Leyton and Koper, 2007). Thus, the prominent features of the uppermost inner core are its isotropy and strong scattering properties. An important open question is to relate these macroscopic properties to the microscopic anisotropy of the iron alloy.

Iron is thought to be the main constituent of Earth's inner core. However, the bulk properties and crystalline structure of Fe at such extreme physical conditions remain uncertain. The hexagonal-close-packed (*hcp*) phase of iron has been proposed as a likely stable phase in the inner core by several authors (e.g. Stixrude and Cohen, 1995; Yoo et al., 1995; Ma et al., 2004) but there is no consensus on its anisotropy (Mao et al., 1998; Steinle-Neumann et al., 2001; Antonangeli et al., 2006). Because the uncertainty on the temperature in the inner core is very large (Williams et al., 1987; Boehler, 1993; Saxena et al., 1994; Ma et al., 2004), other structures such as body-centered cubic (Poirier and Shankland, 1993; Saxena and Dubrovinsky, 1998), double hexagonal closed

packed (Saxena et al., 1995) and orthorhombic (Anderson and Duba, 1997; Andrault et al., 2000) cannot be excluded. The problem is made even more complex by the nature and quantity of light elements present in the inner core (Poirier, 1994). Nickel or silicon may stabilise a body-centered-cubic (*bcc*) phase at inner core conditions (Lin et al., 2002; Vočadlo et al., 2003b; Vočadlo, 2007; Dubrovinsky et al., 2007). A long standing issue in mineral physics is the discrepancy between the Voigt average velocity of iron crystals and the observed seismic velocity. Even the most recent models such as proposed by Vočadlo (2007) and Belonoshko et al. (2007), that incorporate the effect of temperature, have Voigt average shear velocity between 4.0 to 4.4 km.s^{-1}. This is still significantly higher than the adopted 3.5 km.s^{-1} velocity in seismological models.

1.2 Approach of this study

Two distinct classes of model have been proposed to explain the bulk seismic properties of the solid core: (1) Some authors have invoked the presence of elliptic liquid inclusions which could mimic the observed anisotropy and attenuation of seismic waves through the inner core (Singh et al., 2000); (2) Bergman (1997) proposed a solidification texturing model which results in depth dependent anisotropic properties in qualitative agreement with body wave traveltime measurements. In this work, we focus on the specific scattering properties of the uppermost inner core and its implication for the attenuation and velocity dispersion of seismic waves. Previous seismological studies of scattering have thus far only considered the effects of elastically isotropic heterogeneities with possibly anisotropic (anisomeric) spatial distributions

(Cormier et al., 1998; Vidale and Earle, 2000; Cormier and Li, 2002; Cormier, 2007). These seismological models of heterogeneity are not clearly connected with the mineralogical and geodynamical models of the inner core. One may for instance ask: what is the physical meaning of an isotropic velocity perturbation in an intrinsically anisotropic material?

We propose a simple model of solidification texturing of the uppermost inner core, consistent with seismological and mineralogical data. We limit our considerations to a few simple quantities that can be inferred from seismic observations: P and S wave velocities and P-wave attenuation. We model the superficial part of the solid core as an untextured aggregate of iron "patches" (Krasnoshchekov et al., 2005) as depicted in Figure 1. Each patch is characterized by the anisotropic properties of individual iron crystals and the orientation of crystallographic axes varies randomly from one patch to another. One patch is not necessarily made of a single crystal. One can for example imagine that it contains a large number of dendrites with strongly correlated orientation of crystallographic axes. Such a texture is shown in Figure 1 and is similar to what is observed in laboratory experiments of crystallization of ice or *hcp* iron (Worster, 1997; Bergman, 1997; Bergman et al., 2003). The seismic properties of the aggregate depend on the patch size and the iron crystal properties (symmetry, anisotropy). As a consequence of our assumption of random patch orientation, the aggregate is macroscopically isotropic. But, because of crystal anisotropy, seismic wave velocities vary from one patch to an other which makes the aggregate microscopically inhomogeneous. A seismic pulse travelling through such a medium will be prone to amplitude attenuation and velocity dispersion. We show how multiple scattering theory can be used to relate the intrinsic elastic properties of iron crystals to the macroscopic seismic properties of the aggregate. An important

conclusion of our theory is that the Voigt average velocity of a single crystal is a poor approximation of the seismic velocity of the aggregate.

2 Multiple scattering theory

To describe statistically the aggregate, we introduce the following decomposition of the elastic tensor:

$$C_{ijkl}(\mathbf{x}) = C^0_{ijkl} \; + \; \delta C_{ijkl}(\mathbf{x}) \tag{1}$$

$$C^0_{ijkl} = \langle C_{ijkl}(\mathbf{x}) \rangle, \tag{2}$$

where

$$\langle \delta C_{ijkl}(\mathbf{x}) \rangle = 0. \tag{3}$$

Angular brackets represent the ensemble average over all possible orientation of a single crystal, also known as the Voigt average. The fluctuations $\delta C_{ijkl}(\mathbf{x})$ are considered to be single realizations drawn from an ensemble of random fields, having zero mean. In such an aggregate, the spatial variations of the elastic constants are only caused by different orientations of the patches. As usual the material heterogeneity is described by the correlation of the fluctuations, which in our case is a tensor field (Stanke and Kino, 1984):

$$\langle \delta C_{ijkl}(\mathbf{x}) \delta C_{\alpha\beta\gamma\delta}(\mathbf{x}') \rangle \; = \; \Xi^{\alpha\beta\gamma\delta}_{ijkl} \eta(|\mathbf{x} - \mathbf{x}'|), \tag{4}$$

where Ξ denotes the eigth rank covariance tensor of the elastic moduli and depends on the symmetry of the crystal (Hirsekorn, 1988). The function $\eta(x)$ which equals 1 at $x = 0$ and tends to 0 as $x \to \infty$ is the spatial correlation function. It gives the probability that two points separated a distance x from

one another are located within the same patch (Stanke, 1986). Equation (4) reflects two assumptions regarding the statistics of the aggregate: first, there are no orientation correlations between different patches (i.e. there is no macroscopic anisotropy of the aggregate); second, the aggregate is statistically homogeneous. We have chosen a spatial correlation function of the form:

$$\eta(r) \;=\; e^{-r/a}. \tag{5}$$

The correlation function (5) implies that the patches (or grains) are convex and equi-axed, i.e., not elongated in some particular direction. Such a texture would produce anisotropic velocity and attenuation as shown by Margerin (2006). In spite of the limitations mentioned above, an exponential function describes the variable shapes and linear dimensions of grains in a polycrystalline material reasonably well (Stanke, 1986). In this case, the effective average dimension of the patches is $d = 2\,a$.

The inhomogeneity of the aggregate is related to the anisotropy of the patches. For example, if iron is weakly anisotropic, the elastic properties of the medium have only weak variations from patch to patch. The degree of inhomogeneity can be expressed in terms of the effective elastic constants as (Stanke and Kino, 1984):

$$\epsilon^2 \simeq \frac{1}{4}\frac{\langle (C_{IJ} - C^0_{IJ})^2 \rangle}{(C^0_{IJ})^2}. \tag{6}$$

To represent the fourth-order stiffness tensor, we have introduced in equation (6) the Voigt matrix C_{IJ} whose indices I and J vary from 1 to 6 with the following correspondence rule between tensor and matrix indices: (11) $\rightarrow$ 1, (22) $\rightarrow$ 2, (33) $\rightarrow$ 3, (23) $\rightarrow$ 4, (13) $\rightarrow$ 5, (12) $\rightarrow$ 6. The degree of inhomogeneity is defined with $I = J = 3$ for P waves, and with $I = J = 4$ for

S waves.

To calculate the seismic response of the aggregate, we have used a formalism based on the Dyson equation (Rytov et al., 1989) for the ensemble averaged Green function. The theory takes into account all the physics of the problem: arbitrary anisotropy of iron, mode conversions between P and S waves, and multiple scattering (Weaver, 1990). This formalism yields effective phase velocities and spatial decay rates of coherent P and S waves propagating through the aggregate. At a given frequency ω, the seismic coherent field $\langle \mathbf{G} \rangle$ can be decomposed into longitudinal (P) and transverse (S) contributions (Weaver, 1990):

$$\langle \mathbf{G}(\omega, \mathbf{p}) \rangle = g^P(p) \hat{\mathbf{p}}\hat{\mathbf{p}} + g^S(p)(\mathbf{I} - \hat{\mathbf{p}}\hat{\mathbf{p}}), \tag{7}$$

where $g^P(p)$ and $g^S(p)$ are defined as:

$$g^P(p) = \frac{1}{\omega^2 - (pV_0^P)^2 + \sigma^P(p)} \tag{8}$$

$$g^S(p) = \frac{1}{\omega^2 - (pV_0^S)^2 + \sigma^S(p)}. \tag{9}$$

In equation (7), $\mathbf{I}$ is the identity tensor, $\hat{\mathbf{p}}$ is a unit vector in the direction of the wavevector $\mathbf{p}$; V_0^P (V_0^S) and $\sigma^P(p)$ ($\sigma^S(p)$) denote the longitudinal (transverse) Voigt velocity and longitudinal (transverse) mass operator, respectively. The poles of the propagators $g^P(p)$ and $g^S(p)$ give the dispersion relation of P and S waves in the aggregate, respectively (Sheng, 1995). To determine the location of the poles, some approximation of the mass operators has to be made. In the First-Order-Smoothing Approximation, correct to second order in material heterogeneity, Weaver (1990) has shown that $\sigma^P(p)$ and $\sigma^S(p)$ are related to inner products of Ξ with the unit tensor $\mathbf{I}$ and the second rank tensors $\hat{\mathbf{p}}\hat{\mathbf{p}}$. The detailed frequency dependence of the mass operators

is governed by the correlation function η. At sufficiently low frequency, the location of the poles can be given explicitly using the Born approximation which consists in substituting p with $k_0 = \omega/V_0$ in $\sigma(p)$ (Weaver, 1990). One obtains the following expression of the effective wave vector k_e in the untextured aggregate:

$$k_e^{P/S} = \left[\left(\frac{\omega}{V_0^{P/S}} \right)^2 + \frac{\sigma^{P/S}(\omega/V_0^{P/S})}{\left(V_0^{P/S}\right)^2} \right]^{1/2} \tag{10}$$

When the Born approximation fails at high frequencies, one can still locate approximately the pole by calculating the density of states in the random medium. This procedure is described in detail in the book of Sheng (1995), p.85-86. In this work, Born approximation has been used to facilitate calculations and its validity has been verified a posteriori.

The effective velocities $V_e^{P/S}$ and attenuations $\alpha^{P/S}$ of the seismic waves are related to the real and imaginary parts of the mass operators, respectively:

$$\frac{1}{V_e^{P/S}} = \frac{1}{V_0^{P/S}} + \frac{1}{2\,\omega^2\,V_0^{P/S}}\,\Re\{\sigma^{P/S}(\omega/V_0^{P/S})\} \tag{11}$$

$$\alpha^{P/S} = \frac{1}{2\,\omega\,V_0^{P/S}}\,\Im\{\sigma^{P/S}(\omega/V_0^{P/S})\}. \tag{12}$$

Because the material is heterogeneous at the wavelength scale, the effective phase velocity in the aggregate is different from the Voigt velocity. The attenuations $\alpha^{P/S}$ reflect the amplitude decay of the coherent wave caused by scattering. In a recent review paper, Thompson (2002) shows the remarkable agreement between experimental measurements of attenuation in untextured metals and the theoretical prediction (12). To ease the comparison with seismic observations, we define P-wave and S-wave attenuation quality factors as:

$$Q_{P/S} = \frac{\omega}{2\alpha^{P/S}V_0^{P/S}} \tag{13}$$

3 Effective seismic properties of aggregates: study of 6 iron models from the literature

3.1 Anisotropy and Voigt speed of single crystals

Table 1 gives elastic properties of six iron crystals proposed for the inner core, obtained from either laboratory experiments or theoretical calculations. These crystals present very different anisotropic characteristics as revealed by Table 1. For example, the sign and amplitude of the anisotropic parameters for hexagonal iron defined in Appendix A vary significantly from one crystal to an other (Table 1). This is illustrated in Figure 2 where the P and S wave velocities of three hexagonal iron crystals are plotted as a function of the direction of propagation measured from the symmetry axis. In Figure 2a, the longitudinal sound velocity deduced from x-ray diffraction experiments (Mao et al., 1998) has a maximum at 45° from the symmetry axis. This result has not been supported by either first principle calculations or other experimental studies. The theoretical investigations themselves have led to contradictory conclusions: the symmetry axis could be either fast (Laio et al., 2000) or slow (Vočadlo, 2007) as shown in Figure 2. Recently, Dubrovinsky et al. (2007) have proposed that a body-centered-cubic (*bcc*) phase could be stable at inner core conditions. Recent cubic iron models computed by (Belonoshko et al., 2007) and Vočadlo (2007) at inner core temperature, present different anisotropic characteristics, described by the parameter ν in Table 1 (Appendix A). All iron crystals in Table 1 have a higher S-wave Voigt velocity than that inferred from seismology -between 3.5 km.s^{-1} and 3.67 km.s^{-1} in the ak135 model (Kennett et al., 1995) -. Recent theoretical calculations of elastic properties of

iron at inner core conditions converge towards S-wave Voigt velocities between 4.0 km.s^{-1} and 4.4 km.s^{-1}.

3.2 Seismic wave dispersion

We explore the seismic properties of *hcp* and *bcc* iron aggregates at the typical frequency of short period *PKIKP* waves (around 1 Hz). In what follows, an iron model will be simultaneously characterized by its single crystal and aggregate properties. We have calculated the P and S effective velocities for patch sizes ranging from 30 m to 100 km. As explained in section 2, the material heterogeneity induces a shift of the seismic wavespeeds from the Voigt velocities V_0. This effect is illustrated in Figure 3, where we have plotted the normalized variation of phase velocity $\delta V = (V_e - V_0)/V_0$ as a function of adimensional frequency $k_0\, a$ (where k_0 is the Voigt wavenumber and a is the correlation length) for *hcp* aggregates (top) and *bcc* agregates (bottom). Over the whole frequency range, the effective velocity of both P and S waves is reduced compared to the Voigt average. Typically, the shift is stronger by one order of magnitude for S wave than for P wave. For a given polarization the shift grossly increases with the degree of inhomogeneity ϵ^2 (see equation 6), and varies over one order of magnitude at least, depending on the iron models. The effective velocity is also a sensitive function of the size of the patch. The strongest variations occur around $k_0^{S/P} a \approx 1$ which corresponds to a strong coupling between P and S modes. The "jump" of the velocity dispersion curve around $k_0^{S/P} a \approx 1$ is absent in scalar wave propagation and is a remarkable feature of the elastic propagation in metals as illustrated by Stanke and Kino (1984). At very low frequency, our calculations verify the Hashin-Strikman

bounds as they should. Calculations with a gaussian two-point correlation function η yield qualitatively very similar results. Since gaussian correlations are usually too smooth to represent natural materials, we have preferred the more realistic exponential function.

Figure 3 illustrates the renormalization of the velocity in the heterogeneous material. Since the effective seismic velocity of an aggregate is lower than its Voigt average velocity, we can conclude that stable iron phases at inner core condition should have P-wave Voigt velocity close to the observed one, or slightly larger (around 2 %) if the degree of inhomogeneity is large. In the case of S waves, the difference between the Voigt and the seismic velocity has to be positive, and can be large (up to 10 % for the model of Belonoshko et al. (2007)). Our calculations show that the Voigt velocity is not the appropriate parameter to discuss the compatibility of iron models obtained from mineral physics with seismic observations.

3.3 Seismic wave attenuation

We now examine the attenuation properties of six iron aggregates whose properties are summarized in Table 1. In Figure 4 we show the P-wave attenuation $(1/Q_P)$ as a function of adimensional frequency $k_0^P a$. Variations of $1/Q_P$ with respect to adimensional frequency depend on whether ω or a is varied. In our case, we work at constant central frequency $\omega = 2\pi$ and let a range from 300 m to 90 km. A prominent feature is the strong frequency dependence of P-wave attenuation. Typically, the attenuation increases by about two orders of magnitude for P waves as $k_0 a$ varies from 0.1 to 10.

Scattering attenuation is very sensitive to the anisotropic characteristics of iron crystals. For example, the iron models of Mao et al. (1998) and Laio et al. (2000) have nearly equal Voigt velocities for both P and S waves (see Table 1). However, the elastic anisotropy of the crystals is quite different as illustrated in Figure 2. As a consequence, we find one order of magnitude difference for P-wave attenuation in the aggregates, at fixed patch size. At high frequency, we observe that longitudinal attenuation increases with the degree of inhomogeneity ϵ_P^2. All the attenuation curves show a smooth bump around $k_0 a = 1$, which corresponds to a frequency range where the coupling between P and S waves is maximum. Because attenuation and velocity are related by Kramers-Krönig relations, the "jump" of the velocity curve and the "bump" of the attenuation curve coincide. Considering these six iron models proposed for the inner core, we find as much as two orders of magnitude difference in attenuation for P waves at fixed patch size. Elastic wave attenuation is therefore an important quantity to characterize the properties of iron in the inner core.

In Figure 4, the grey lines give some typical values for P-wave attenuation at 1 Hz at the top of the inner core, i.e. $300 < Q_P < 600$ as proposed by Yu and Wen (2006). Several iron models can explain the observed Q_P by scattering attenuation only, but with different textures. For example, the Belonoshko et al. (2007) model yields typical size of patches of about a few hundred meters, whereas the *bcc* iron model at 5500 K by Vočadlo (2007) implies patches around ten kilometers. In the case of Laio et al. (2000), it seems difficult to explain P-wave attenuation in the uppermost inner core by scattering only. The study of these six iron models reveals a clear trade-off between elastic properties and typical size of patches (scattering objects). In what follows, this problem will

be further examined in order to simultaneously constrain crystal anisotropy and the texture of aggregates in the uppermost inner core.

4 Constraints on elastic contants of iron in the inner core

In this section, we consider the following inverse problem: find iron models that match the seismic measurements of P and S wave velocities, and P wave attenuation at 1 Hz in the uppermost inner core. An iron model is defined by the elastic tensor of a single crystal and the texture of the aggregate. Because the stable phase of iron at inner core conditions is still uncertain, we propose to examine two kinds of crystal symmetry: hexagonal and cubic. In our simple model, the texture is characterized by the correlation length a, equal to half the average patch size. We let a vary over more than two orders of magnitude: 50 m $< a <$ 10000 m.

The observation of strong $PKiKP$ coda suggests that scattering attenuation is the dominant mechanism for attenuation in the inner core. This interpretation is also supported by the study of Cormier and Li (2002) and Cormier (2007). A commonly accepted value for Q_P at the top of the inner core is about 300 (Yu and Wen, 2006). We impose that an acceptable iron model should have a scattering Q_P within the range 300-600. This choice implies that more than half the observed attenuation is explained by scattering and leaves some room for other attenuation mechanisms. Since S-wave attenuation in the inner core around 1 Hz is still poorly known, we do not impose constraints on Q_S. The range of acceptable seismic velocities corresponds to the values given by the ak135 model for the whole inner core.

4.1 Hexagonal iron

To find acceptable iron models we perform a systematic grid search in the C_{IJ} space. Only positive definite elastic tensors have been retained. For each correlation length, we test 1.8×10^8 physical iron models with anisotropy parameters $(\varepsilon, \delta, \gamma)$ smaller than 50%. In Figure 5 (left), we represent the percentage of acceptable hexagonal models as a function of the correlation length. The curve shows a sharp maximum at $a \simeq 220$ m, which yields an average size of the patches around 450 m. The correlation length of the aggregate cannot be smaller than 140 m but can be as large as 10000 m. It is to be noted that the most probable patch size is about 20 times smaller than the central wavelength of P waves. A careful analysis reveals that the bounds on the seismic velocities determine the overall number of acceptable models, whereas the bounds on the attenuation fix the position of the maximum.

For three correlation lengths a =140 m, 220 m, 1000 m, we examine in Figure 6 the distribution of acceptable models in the (ε, δ) parameter space. We focus on the two parameters controlling the P-wave crystal anisotropy, in order to facilitate comparisons with results from mineral physics. Figure 6 is a 2-D histogram of the number of acceptable models. For each correlation length, there is a clear trade-off between ε and δ because only three independent observations serve to constrain 5 independent parameters. To avoid artefacts due to uneven sampling of the model space, we have taken care of normalizing the results by the total number of tested models per class. In fact the systematic exploration of the C_{IJ} space yields relatively homogeneous coverage of the (ε, δ) space. In Figure 7, we show the a-posteriori histograms of acceptable Voigt velocities for the three correlation lengths.

At small correlation length ($a = 140$ m), the aggregate is most likely composed of hexagonal iron crystals with a slow symmetry axis ($20\% < \varepsilon < 50\%$), and possibly high Voigt velocities (11.6 km.s^{-1}< V_0^P <12.1 km.s^{-1}, 3.8 km.s^{-1}< V_0^S <4.7 km.s^{-1}). There is no clear constraint on δ. We remark that Voigt velocities of iron crystals can never be smaller than seismic velocities, but high Voigt velocities are not necessarily incompatible with seismic observations.

At large correlation length ($a > 500$ m), the (ε , δ) distribution has the shape of an ellipse centered around $(0, 0)$, with positive correlation between ε and δ in the range $-10\% < \varepsilon < 10\%$, $-20\% < \delta < 25\%$. The crystal Voigt velocities must be close to seismic velocities. Careful analysis shows that there are slightly more *hcp* crystals with a slow symmetry axis, than with a fast symmetry axis. At large correlation length, none of the 8 hexagonal iron models considered in this study has both anisotropic parameters and Voigt velocities compatible with seismic observations.

For $a \sim 220$ m, we obtain a maximum of acceptable iron aggregates. Corresponding iron crystals have a complex distribution in ε and δ. δ is not constrained, and ε varies between -20% and $+50\%$. Interestingly, the elliptic domain which defined acceptable models at large correlation length is forbidden when a equals the most probable patch size. Like for small correlation lengths, we obtain a larger number of hexagonal iron crystals with a slow symmetry axis for P waves. The distributions of acceptable P-wave Voigt velocity (11.3 km.s^{-1}< V_0^P <12.0 km.s^{-1}) and S-wave Voigt velocity (3.5 km.s^{-1}< V_0^S <5.5 km.s^{-1}) are very broad, with an average clearly higher than the seismic velocities. The iron crystal proposed by Steinle-Neumann et al. (2001) is the only model which presents both anisotropic parameters (ε, δ) and Voigt velocities that are compatible with seismic observations. However, this iron model is questionable

because of the too large value of the axial ratio of *hcp* iron predicted by the calculations (Gannarelli et al., 2005).

4.2 Cubic iron

We perform a grid search in the $(C_{11}, C_{12}, C_{44})/\rho$ parameter space, where ρ is the model iron density. The normalization by ρ facilitates the comparison between models with different densities. In any case, the scattering properties of an aggregate depend only on C_{IJ}/ρ.

For a given texture, we test 8.8×10^6 cubic iron crystals with a homogeneous distribution in the range: $0.1 < C_{11}/\rho < 0.2$, $0.06 < C_{12}/\rho < 0.12$, $0 < C_{44}/\rho < 0.04$, where the C_{IJ} and ρ units are GPa and kg.m^{-3}, respectively. In Figure 5 (right), we represent the percentage of acceptable cubic models as a function of the correlation length. The curve shows a maximum at $a \simeq 200$ m, which yields an average size of the patches around 400 m. Therefore the most probable size of patch is a robust feature, independent of the symmetry of the crystal. Like in the hexagonal case, the correlation length of the aggregate cannot be smaller than 150 m but can be as large as 10000 m. The percentage of accepted models is by one order of magnitude smaller in the cubic case than in the hexagonal case.

For three correlation lengths (150 m, 200 m and 500 m), we examine, in Figure 8, the distribution of elastic constants of acceptable cubic crystals. At large correlation length, we observe two distinct families shown in grey and black in Figure 8 (middle-bottom), whereas a single family exists at correlation length smaller than 200 m. The black and white circles show the recent results of

Vočadlo (2007) for cubic iron at two different inner core temperatures, and the black square is the recent *bcc* iron model by Belonoshko et al. (2007). This last model is completely compatible with seismic observations and corresponds to the "grey" family of cubic models.

In Figure 9, we show the a posteriori distributions of Voigt velocities for three correlation lengths. The main features are very similar to the hexagonal case but the bounds are slightly sharper. For the most probable patch size, the average *S*-wave Voigt velocity is around 4.4 km.s^{-1}, in agreement with recent results by Vočadlo (2007) and Belonoshko et al. (2007). Our study shows that some cubic iron crystal with S-wave Voigt velocity around 4.0 km.s^{-1} can explain seismological data without invoking the presence of melt, as for example the iron model by Belonoshko et al. (2007). On the other hand the *bcc* iron model at $5500K$ by Vočadlo (2007), although in reasonably good agreement with the results of our inversion, is not anisotropic enough to induce a strong renormalization of the seismic velocities in the aggregate (only 1 % as shown in Figure 3). For such an iron model, it is necessary to invoke the presence of some melt to explain the seismic velocities.

5 Discussion and conclusion

5.1 Patch size

(1) From mineral physics and geodynamics. Estimates of the size of iron crystals in the Earth's inner core vary from the entire volume, some 1200 km, to about 5 mm. Stixrude and Cohen (1995) have proposed that a single crystal of iron with anisotropy around 4 % could explain seismic traveltimes. The

smaller estimates stem from geodynamical considerations. Near the melting temperature of iron, a grain size of about 5 mm is necessary to make the viscosity smaller than 10^{16} Pa.s, as proposed by Buffett (1997). Assuming dynamic recrystallisation, Yoshida et al. (1996) obtained a typical crystal size around 5 m. Bergman (1997, 1998) suggested that observed attenuation and velocity anisotropy of the inner core may result from radially elongated columnar grains and estimated the columnar grain width around 200 m. This last study is in good agreement with our most probable patch size.

(2) From seismology. With scattering and a fabric interpretation of seismic attenuation, Cormier and Li (2002) have proposed average scale length of isotropic heterogeneities around 10 km, and P-wave velocity perturbations around 8.4% from the centre of the inner core to about 1000 km radius. From the energy envelopes of $PKiKP$ coda waves, Vidale and Earle (2000) have obtained a scale length of about 2 km, and elastic moduli fluctuations of 1.2% in the uppermost 300 km of the inner core. These results may reflect a trade-off between velocity perturbations and scale length. However, the most serious criticism is the lack of physical connection between the hypothesized isotropic seismic heterogeneities and the crystalline nature of the inner core. Our most probable correlation length (around 200m) is smaller than previous estimates by Cormier and Li (2002) and Vidale and Earle (2000), but is close to the lower limit proposed by Cormier et al. (1998) (about 15 % P-wave perturbations and scale length in the range 0.5-2 km).

5.2 On the presence of melt

The vast majority of proposed iron models for the inner core displays much higher Voigt average velocities than what is inferred from seismic traveltimes. This discrepancy has sometimes been used as an argument to support the presence of liquid in the inner core (Singh et al., 2000; Vočadlo, 2007). In our study, we have shown that high Voigt velocities, typically of the order of what is found in the most recent studies (Belonoshko et al., 2007; Vočadlo, 2007), do not necessarily imply the presence of melt. The reason is that the effective velocity in an aggregate can be as much as 15 % smaller (according to the anisotropic characteristics of iron crystal) than the average velocity in a single crystal. Two additional points have to be noted: (1) Iron crystals with Voigt velocities smaller than seismic wavespeeds have to be rejected, independent of our assumption for the value of Q (2) Iron models with Voigt velocities larger than 5.5km.s^{-1} can also be clearly rejected, unless they contain a huge amount of melt, typically more than 20 % according to Figure 2 in Singh et al. (2000).

5.3 Cubic vs Hexagonal

Most theoretical and experimental studies show that hexagonal metals at ambient temperature have a fast symmetry axis (Antonangeli et al., 2006). But the effect of temperature on the elastic constants is still debated (Laio et al., 2000). We found that *hcp* iron models with a slow symmetry axis are more probable in the inner core. If further experimental or theoretical investigations definitely show that *hcp* iron at inner core conditions has a fast symmetry axis, we may conclude on the basis of our uppermost inner core model that

the stable iron phase is unlikely to be hexagonal. Recent cubic models from the literature are in very good agreement with the results of our inversion. Therefore, our study supports a stable *bcc* iron phase in the inner core, as proposed by Dubrovinsky et al. (2007).

Although our study provides some indications on the possible elastic constants of iron, some large uncertainties remain. They are clearly caused by a lack of seismological constraints. In future studies, the modeling of the following three observations could significantly reduce the uncertainties on the properties of iron in the inner core: (1) energy envelope of PKiKP coda; (2) direct measurements of Q_S at 1 Hz; (3) velocity and attenuation anisotropy in the bulk of the inner core. As a large number of records of *PKiKP* coda are available, for which multiple scattering may be relevant, we plan to focus our efforts on this aspect in future works. The modelling of frequency dependent inner core attenuation combined with coda analysis could unravel the relative contributions of viscoelasticity and scattering attenuation.

References

Anderson, O. L., Duba, A., 1997. Experimental melting curve of iron revisited. J. Geophys. Res. 102, 22659–22669.

Andrault, D., Fiquet, G., Charpin, T., Bihan, T. L., 2000. Structure analysis and stability field of β-iron at high P and T. Am. Mineral. 85, 364–371.

Antonangeli, D., Merkel, S., Farber, D. L., 2006. Elastic anisotropy in hcp metals at high pressure and the sound wave anisotropy of the earth's inner core. Geophys. Res. Lett. 33, doi:10.1029/2006GL028237.

Beghein, C., Trampert, J., 2003. Robust normal mode contraints on inner-core

anisotropy from model space search. Science 299, 552–555.

Belonoshko, A. B., Skorodumova, N. V., Davis, S., Osiptsov, A. N., Rosengren, A., Johansson, B., 2007. Origin of the low rigidity of the Earth's inner core. Science 316, 1603–1605.

Bergman, M. I., 1997. Measurements of electric anisotropy due to solidification texturing and the implications for the Earth's inner core. Nature 389, 60–63.

Bergman, M. I., 1998. Estimates of earth's inner core grain size. Geophys. Res. Lett. 25, 1593–1596.

Bergman, M. I., Agrawal, S., Carter, M., Macleod-Silberstein, M., 2003. Transverse solidification textures in hexagonal close-packed alloys. J. Cryst. Growth 255, 204–211.

Boehler, R., 1993. Temperatures in the Earth's core from melting-point measurements of iron at high static pressures. Nature 363, 534–536.

Bréger, L., Romanowicz, B., Tkalčić, H., 1999. PKP(BC-DF) traveltime residuals and short period heterogeneity in the deep earth. Geophys. Res. Lett. 26, 3169–3172.

Buffett, B. A., 1997. Geodynamics estimates of the viscosity of the Earth's inner core. Nature 402, 571–573.

Calvet, M., Chevrot, S., Souriau, A., 2006. P-wave propagation in transversely isotropic media - II . Application to inner core anisotropy: Effects of data averaging, parametrization and a priori information. Phys. Earth Planet. Int. 156, 21–40.

Cao, A., Romanowicz, B., 2004. Hemispherical transition of seismic attenuation at the top of the earths inner core. Earth Planet. Sci. Lett. 228, 243–253.

Cormier, V. F., 2007. Texture of the uppermost inner core from forward- and back-scattered seismic waves. Earth Planet. Sci. Lett.

doi:10.1016/j.epsl.2007.04.003.

Cormier, V. F., Li, X., 2002. Frequency-dependent seismic attenuation in the inner core. II. A scattering and fabric interpretation. J. Geophys. Res. 107, doi:10.1029/2002JB001796.

Cormier, V. F., Xu, L., Choy, G. L., 1998. Seismic attenuation of the inner core: Viscoelastic or stratigraphic? Geophys. Res. Lett. 25, 4019–4022.

Creager, K. C., 1999. Large-scale variations in inner core anisotropy. J. Geophys. Res. 104, 23127–23139.

Dubrovinsky, L., N. Dubrovinskaia, O. N., Kantor, I., Kuznetzov, A., Prakapenka, V. B., Vitos, L., Johansson, B., Mikhaylushkin, A. S., Simak, S. I., Abrikosov, I. A., 2007. Body-centered cubic iron-nickel alloy in earth's core. Science 316, 1880–1883.

Gannarelli, C. M. S., Alfè, D., Gillan, M. J., 2005. The axial ratio of hcp iron at the conditions of the Earth's inner core. Phys. Earth Planet. Int. 152, 67–77.

Garcia, R., 2002. Constraints on uppermost inner core structure from waveform inversion of core phases. Geophys. J. Int. 150, 651–664.

Garcia, R., Souriau, A., 2000. Inner core anisotropy and heterogeneity level. Geophys. Res. Lett. 27, 3121–3124.

Hirsekorn, S., 1988. The scattering of ultrasonic waves by multiphase polycristals. J. Acoust. Soc. Am. 83, 1231–1241.

Ishii, M., Dziewonski, A. M., 2002. The innermost inner core of the earth: Evidence for a change in anisotropic behavior at the radius of about 300 km. Proc. Natl. acad. Sci. U.S.A. 22, 14026–14030.

Kennett, B. L. N., Engdahl, E. R., Buland, R., 1995. Constraints on seismic velocities in the earth from traveltimes. Geophys. J. Int. 122, 108–124.

Koper, K., Franks, J. M., Dombrovskaya, M., 2004. Evidence for small-scale

heterogeneitiy in Earth's inner core from a global study of PKiKP coda waves. Earth Planet. Sci. Lett. 228, 227–241.

Krasnoshchekov, D. N., Kaazik, P. B., Ovtchinnikov, V. M., 2005. Seismological evidence for mosaic structure of the surface of the earth's inner core. Nature 435, 483–487.

Laio, A., Bernard, S., Chiarotti, G. L., Scandolo, S., Tosatti, E., 2000. Physics of iron at Earth's core conditions. Science 287, 1027–1030.

Leyton, F., Koper, K. D., 2007. Using PKiKP coda to determine inner core structure: 2. Determination of Q_c. J. Geophys. Res. 112, doi:10.1029/2006JBOO4370.

Li, X., Cormier, V. F., 2002. Frequency dependent attenuation in the inner core: Part I. A viscoelastic interpretation. J. Geophys. Res. 107, doi:10.1029/2002JB001795.

Lin, J. F., Heinz, D. L., Campbell, A. J., Devine, J. M., Shen, G., 2002. Iron-Silicon alloy in the Earth's core? Science 295, 313–315.

Ma, Y., Somayazulu, M., Shen, G., Mao, H., Shu, J., Hemley, R., 2004. In situ X-ray diffraction studies of iron to Earth core conditions. Phys. Earth Planet Inter. 143–144, 455–467.

Mao, H. K., Shu, J., Shen, G., Hemley, R. J., Li, B., Singh, A. K., 1998. Elasticity and rheology of iron above 220 GPa and the nature of the earth's inner core. Nature 396, 741–743 (Correction, Nature 399, 280, 1999.).

Margerin, L., 2006. Attenuation, transport and diffusion of scalar waves in textured random media. Tectonophysics 416, 229–244.

Mensch, T., Rasolofosaon, P., 1997. Elastic-wave velocities in anisotropic media of arbitrary symmetry— generalization of Thomsen's parameters ϵ, δ and γ. Geophys. J. Int. 128, 43–64.

Niu, F., Wen, L., 2001. Hemispherical variations in seismic velocity at the top

of the Earth's inner core. Nature 410, 1081–1084.

Poirier, J.-P., 1994. Light elements in the Earth's outer core : a critical review. Phys. Earth Planet. Inter. 85, 319–337.

Poirier, J.-P., Shankland, T. J., 1993. Dislocation melting of iron and the temperature of the inner core boundary, revisited. Geophys. J. Int. 115, 147–151.

Poupinet, G., Kennett, B. L. N., 2004. On the observation of PKiKP and its high frequency coda on the Warramunga array, Australia. Phys. Earth Planet. Inter. 146, 497–512.

Rytov, S. M., Kravtsov, Y. A., Tatarskii, V. I., 1989. Principles of Statistical Radiophysics. Vol. 4. Springer-Verlag New York.

Saxena, S. K., Dubrovinsky, L. S., 1998. Thermodynamics of iron phases at high pressure and temperature. In: Manghanani, L. S., Yagi, T. (Eds.), Properties of Earth and Planetary materials at high pressure ans temperature. American Geophysical Union, pp. 271–279.

Saxena, S. K., Dubrovsky, L. S., Häggkvist, P., Cerenius, Y., Shen, G., Mao, H. K., 1995. Synchrotron X-ray Study of Iron at High Pressure and Temperature. Science 269, 1703–1704.

Saxena, S. K., Shen, G., Lazor, P., 1994. Temperatures in Earth's core based on melting and phase transformation experiments on iron. Science 264, 405–407.

Shearer, P. M., 1994. Constraints on inner core anisotropy from PKP(DF) travel times. J. Geophys. Res. 99, 19647–19659.

Sheng, P., 1995. Introduction to Wave Scattering, Localization and Mesoscopic Phenomena. Academic Press, San Diego.

Singh, S. C., Taylor, M. A. J., Montagner, J. P., 2000. On the presence of liquid in earth's inner core. Science 287, 2471–2474.

Söderlind, P., Moriarty, J. A., Willis, J. M., 1996. First principles theory of iron up to Earth-core pressure: structural, vibrational, and elastic properties. Phys. Rev B 53, 14063–14072.

Souriau, A., Roudil, P., 1995. Attenuation in the uppermost inner core from broad-band GEOSCOPE PKP data. Geophys. J. Int 123, 572–587.

Stanke, F. E., 1986. Spatial autocorrelation functions for calculations of effective propagation constants in polycristalline materials. J. Acoust. Soc. Am. 80, 1479–1485.

Stanke, F. E., Kino, G. S., 1984. A unified theory for elastic wave propagation in polycristalline materials. J. Acoust. Soc. Am. 75, 665–681.

Steinle-Neumann, G., Stixrude, L., Cohen, R. E., 1999. First-principles elastic constants for the hcp transition metals Fe, Co and Re at high pressure. Phys. Rev. B 60, 791–799.

Steinle-Neumann, G., Stixrude, L., Cohen, R. E., Gülseren, O., 2001. Elasticity of iron at the temperature of the earth's inner core. Nature 413, 47–60.

Stixrude, L., Cohen, R. E., 1995. High pressure elasticity of iron and anisotropy of Earth's inner core. Science 267, 1972–1975.

Stroujkova, A., Cormier, V. F., 2004. Regional variations in the uppermost 100 km of the earth's inner core. J. Geophys. res. 109, doi:10.1029/2004JB002976.

Su, W.-J., Dziewonski, A. M., 1995. Inner core anisotropy in three dimensions. J. Geophys. Res. 100, 9831–9852.

Thompson, B., 2002. Elastic-wave propagation in random polycrystals: fundamentals and application to nondestructive evaluation. In: Fink, M., Kuperman, W., Montagner, J.-P., Tourin, A. (Eds.), Imaging of complex media with acoustic and seismic waves. Vol. 84 of Topics in applied physics. Springer-Verlag Berlin Heidelberg, pp. 233–256.

Vidale, J. E., Earle, P. S., 2000. Fine-scale heterogeneity in the Earth's inner core. Nature 404, 273–275.

Vočadlo, L., 2007. Ab initio calculations of the elasticity of iron and iron alloys at inner core conditions: Evidence for a partially molten inner core? Earth Planet. Sci. Lett. 254, 227–232.

Vočadlo, L., Alfé, D., Gillan, M. J., Price, G. D., 2003a. The properties of iron under core conditions from first principles calculations. Phys. Earth Planet. Int. 140, 102–125.

Vočadlo, L., Alfé, D., Gillan, M. J., Wood, I. G., Brodholt, J. P., Price, G. D., 2003b. Possible thermal and chemical stabilization of body-centered-cubic iron in the Earth's core. Nature 424, 536–539.

Weaver, R. L., 1990. Diffusivity of ultrasound in polycrystals. J. Mech. Phys. Solids 38, 55–86.

Wen, L., F. Niu, F., 2002. Seismic velocity and attenuation structures in the top of the earths inner core. J. Geophys. Res. 107, doi:10.1029/2001JB000170.

Williams, Q., Jeanloz, R., Bass, J., Svendsen, B., Ahrens, T. J., 1987. The melting curve of iron to 250 Gigapascals: a constraint on the temperature at Earth's center. Science 236, 181–182.

Worster, M. G., 1997. Convection in mushy layers. Annu. Rev. Fluid Mech. 29, 91–122.

Yoo, C. S., Akella, J., Campbell, A. J., Mao, H. K., Hemley, R. J., 1995. Phase diagram of iron by in situ X-ray diffraction: implications for Earth's core. Science 270, 1473–1475.

Yoshida, S., Sumita, I., Kumazawa, M., 1996. Growth model of the inner core coupled with the outer core dynamics and the resulting elastic anisotropy. J. Geophys. Res. 101, 28085–28103.

Yu, W., Wen, L., 2006. Seismic velocity and attenuation structures in the top 400 km of the Earth's inner core along equatorial paths. J. Geophys. Res. 111, doi:10.1029/2005JB003995.

A Anisotropic parameters for hexagonal and cubic crystals

A.1 Hexagonal symmetry

In a transversely isotropic medium (hexagonal symmetry), the symmetry axis defines a particular direction which is usually chosen along the $\hat{\mathbf{x}}_3$-axis for convenience. To describe anisotropic properties of hexagonal crystals, Mensch and Rasolofosaon (1997) have defined three anisotropic parameters:

$$\begin{aligned} \varepsilon &= \frac{(C_{11} - C_{33})}{2C_{33}} \\ \delta &= \frac{(C_{13} - C_{33} + 2C_{44})}{C_{33}} \\ \gamma &= \frac{(C_{66} - C_{44})}{2C_{44}} \end{aligned} \tag{A.1}$$

The parameter ε represents P-wave anisotropy *i.e.* the difference between the phase velocities perpendicular and parallel to the symmetry axis. A negative value of ε corresponds to a fast symmetry axis for P waves (Table 1). The parameter γ represents the anisotropy of S waves in a similar way. The parameter δ controls P wave propagation at intermediate angles from the symmetry axis. In order to fully prescribe the elastic properties of hexagonal crystals, two additional parameters have to be introduced. We have chosen the P and S Voigt average velocities because they are routinely compared with the seismic measurements.

A.2 Cubic symmetry

The stiffness tensor of a cubic crystal is described by three independant constants C_{11}, C_{12} and C_{44}. The invariant anisotropy factor for cubic-class crystal is defined as:

$$\nu = C_{11} - C_{12} - 2C_{44} \tag{A.2}$$

The elastic properties of cubic crystal are fully described by the parameter ν and the P and S Voigt average velocities.

Hexagonal Iron Models	ρ	C_{11}	C_{12}	C_{44}	C_{33}	C_{13}	V_0^P	V_0^S	ν	ε	δ	γ	ϵ_P	ϵ_S
	($kg.m^{-3}$)	(GPa)	(GPa)	(GPa)	(GPa)	(GPa)	(km.s^{-1})	(km.s^{-1})	(GPa)	(%)	(%)	(%)	(%)	(%)
HCP Iron														
Mao et al. (1998)	12600	1533	367	583	1544	835	11.47	5.92		-0.36	+29.60	-20.50	2.46	8.71
Laio et al. (2000)	12885	1697	809	444	1799	757	11.45	5.90		-2.84	-11.12	+2.73	0.80	1.75
Vočadlo (2007)	13155	1311	159	1642	1642	1074	11.14	4.04		+2.84	-15.22	+15.72	2.22	5.17
BCC Iron														
Belonoshko et al. (2007)	13850	1561	1448	365			11.54	4.20	-617				2.79	17.53
Vočadlo (2007)	13155	1603	1258	256			11.29	4.11	-167				0.86	4.91
Vočadlo (2007)	13842	1795	1519	323			11.83	4.24	-370				1.60	9.73

Table 1

Elastic properties of hexagonal (*hcp*) and cubic (*bcc*) iron crystals and associated untextured aggregate: density (ρ), elastic constants (C_{IJ}), hexagonal anisotropic parameters (ε,δ,γ), cubic anisotropic parameter (ν), *P*-wave and *S*-wave Voigt velocities (V_0^P, V_0^S), degrees of inhomogeneity (ϵ_P^2,ϵ_S^2). The iron models have been computed at inner core temperature except Mao et al. (1998) and Laio et al. (2000).

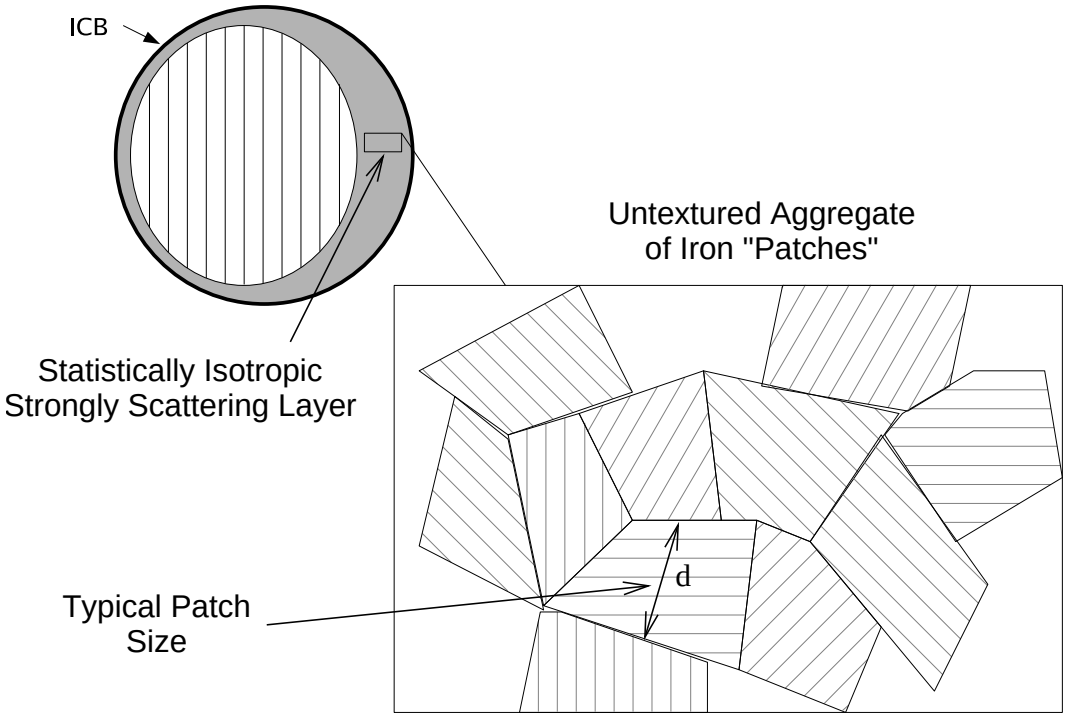

Fig. 1. Modelling of the superficial layer at the top of the solid inner core as an untextured aggregate of iron "patches", with typical size d. ICB: Inner Core Boundary.

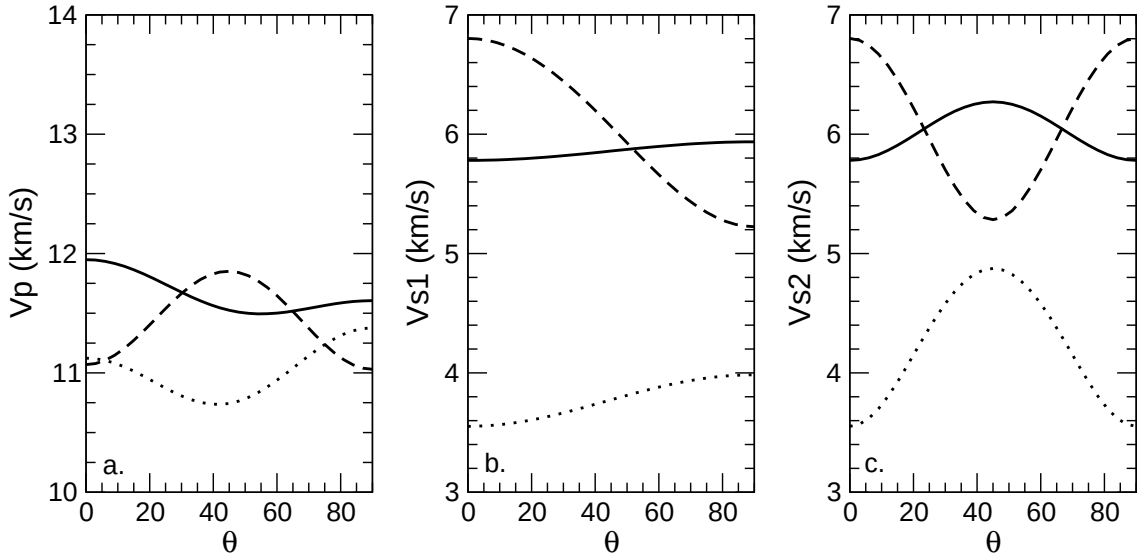

Fig. 2. *P*-wave velocity (a) and *S*-wave velocities (b and c) in a single crystal of iron as a function of propagation direction with respect to symmetry axis, for 3 iron models: Laio et al. (2000) (solid line), Mao et al. (1998) (dashed line) and Vočadlo (2007) (dotted line). θ is the angle between the direction of propagation and the symmetry axis of the crystal.

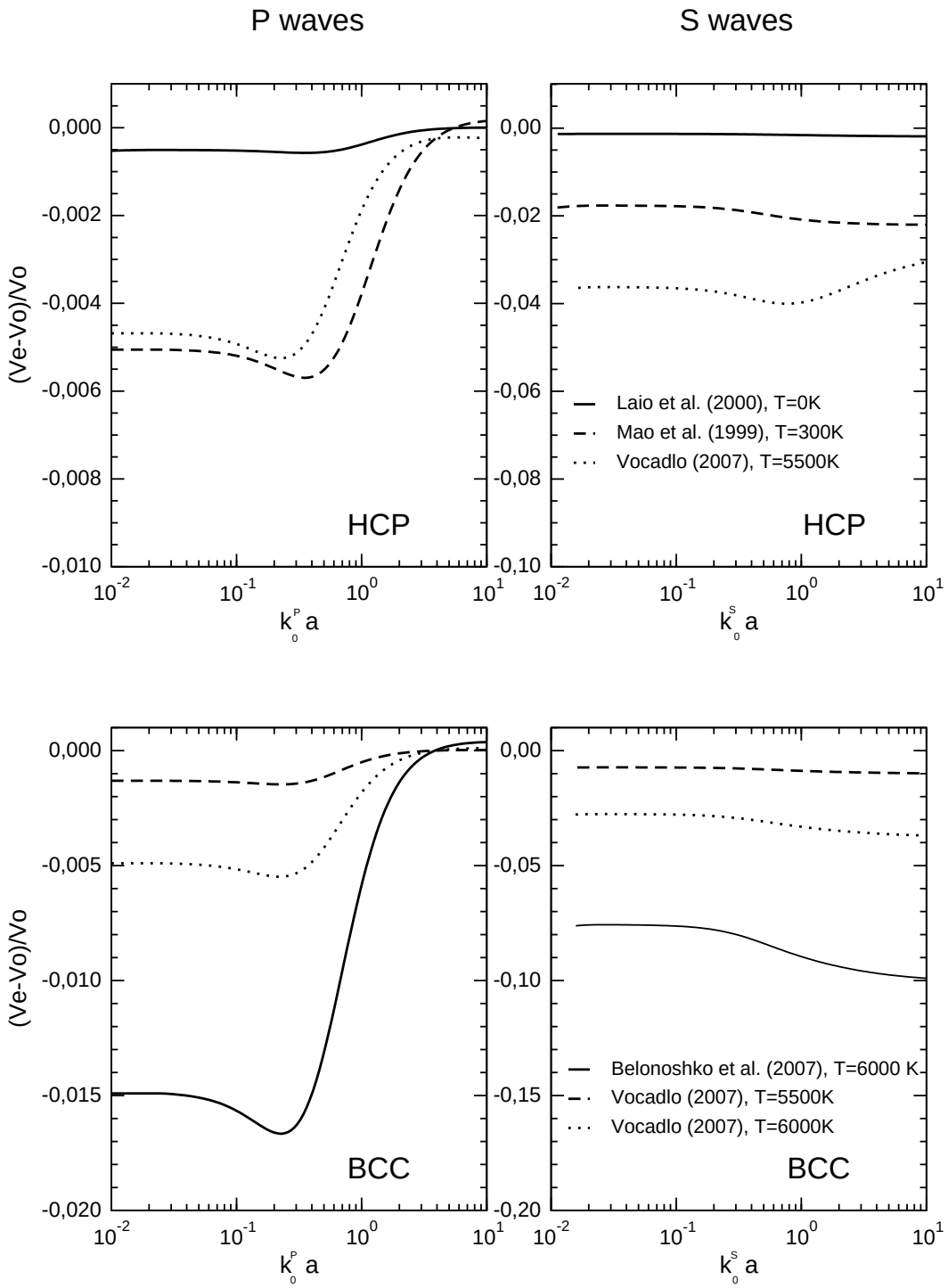

Fig. 3. Normalized variations of longitudinal-wave (left) and transverse-wave (right) phase velocities in hexagonal iron aggregates (top) and in cubic iron agregates (bottom) as a function of adimensional frequency $k_0\,a$. k_0 and V_0 are the Voigt wave vector and velocity respectively, V_e is the effective velocity in the aggregate, and a is the correlation length.

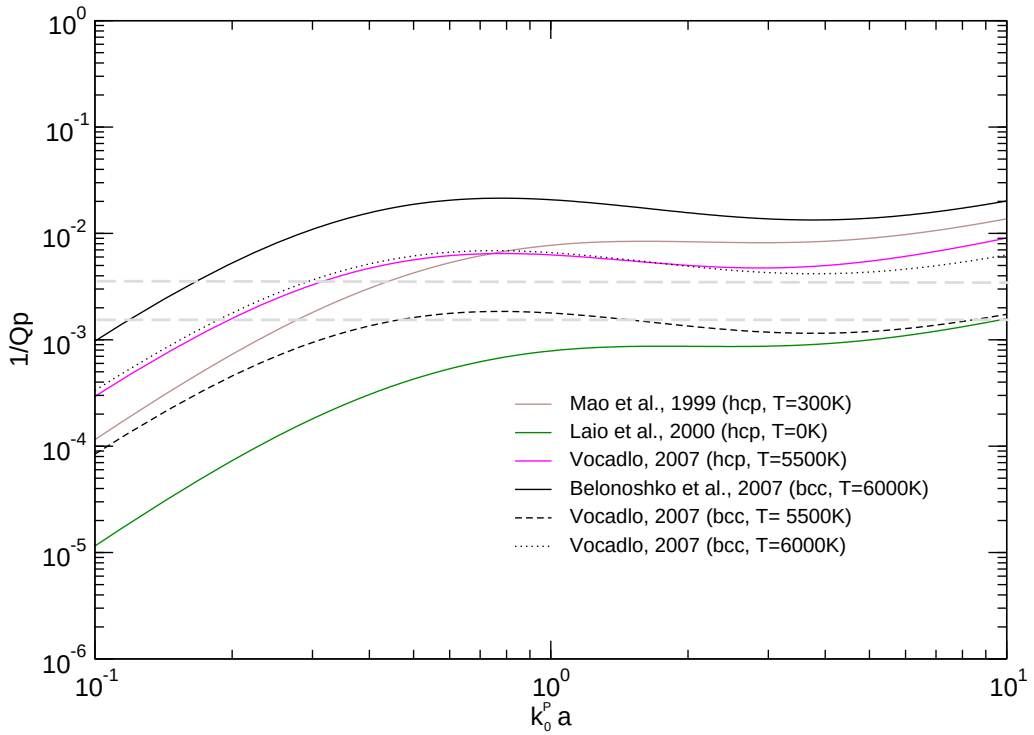

Fig. 4. P-wave attenuation $(1/Q_P)$ as a function of adimensional frequency $k_0\, a$. Amplitude attenuation is computed for three hexagonal iron models and three cubic iron models proposed for the inner core. The grey dashed lines correspond to $Q_P = 300$ and $Q_P = 600$.

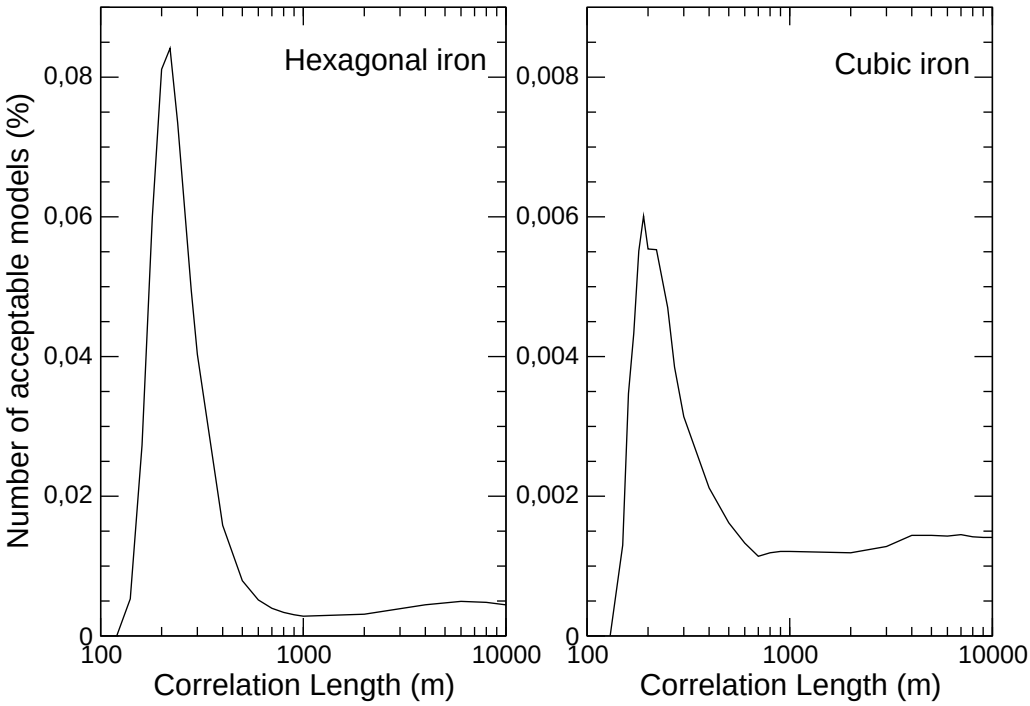

Fig. 5. Number of acceptable iron crystals as a function of the correlation length: hexagonal symmetry (left) and cubic symmetry (right). The corresponding aggregates verify the seismic observations at 1 Hz: P-wave and S-wave velocities are in the range of the ak 135 model of the whole inner core, and attenuation quality factor Q_P lies between 300 and 600.

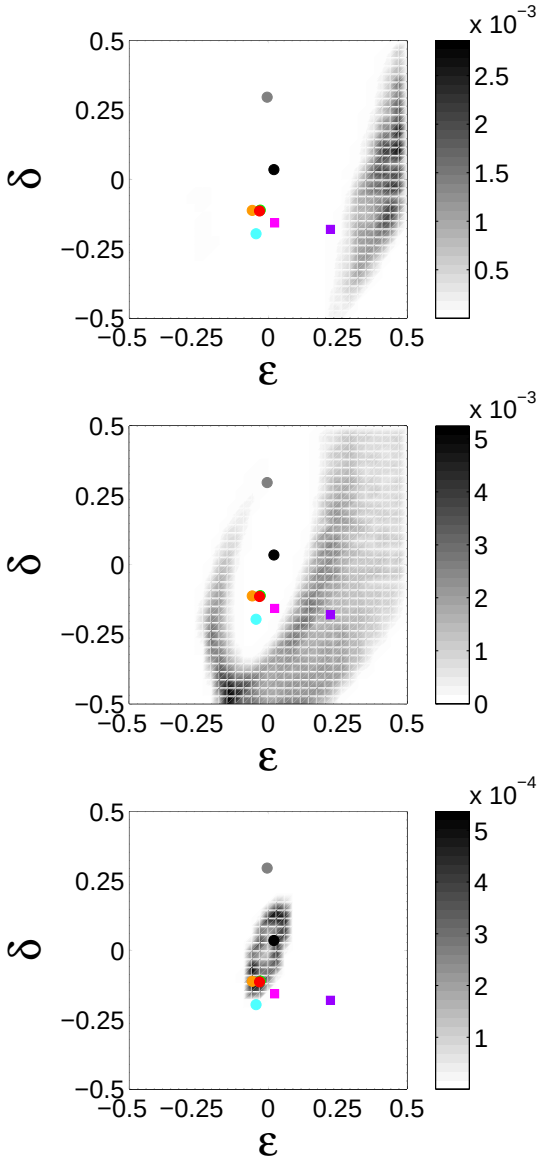

Fig. 6. Density of acceptable hexagonal crystals as a function of the anisotropic parameters ε and δ, for $a = 140$ m (top), $a = 220$ m (middle) and $a = 1000$ m (bottom). For comparison, color dots representing eight *hcp* iron models are plotted: Stixrude and Cohen (1995) (red), Söderlind et al. (1996) (black), Mao et al. (1998) (brown), Steinle-Neumann et al. (1999) (cyan), Laio et al. (2000) (green), Steinle-Neumann et al. (2001) (purple), Vočadlo et al. (2003a) (orange), Vočadlo (2007) (magenta). Only two models have been computed at inner core temperature (squares).

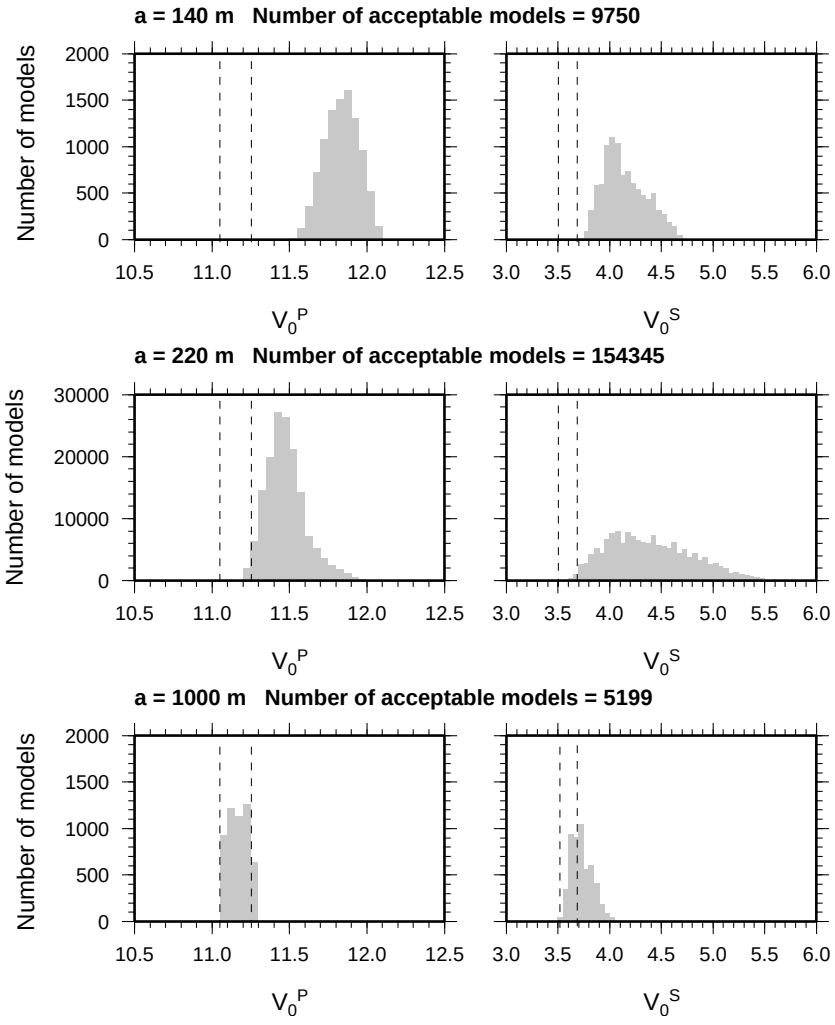

Fig. 7. Distribution of Voigt velocities of acceptable *hcp* iron crystals for different correlation lengths: $a = 140$ m, $a = 220$ m, $a = 1000$ m (from top to bottom). Vertical lines delimit the range of seismic velocities in the inner core.

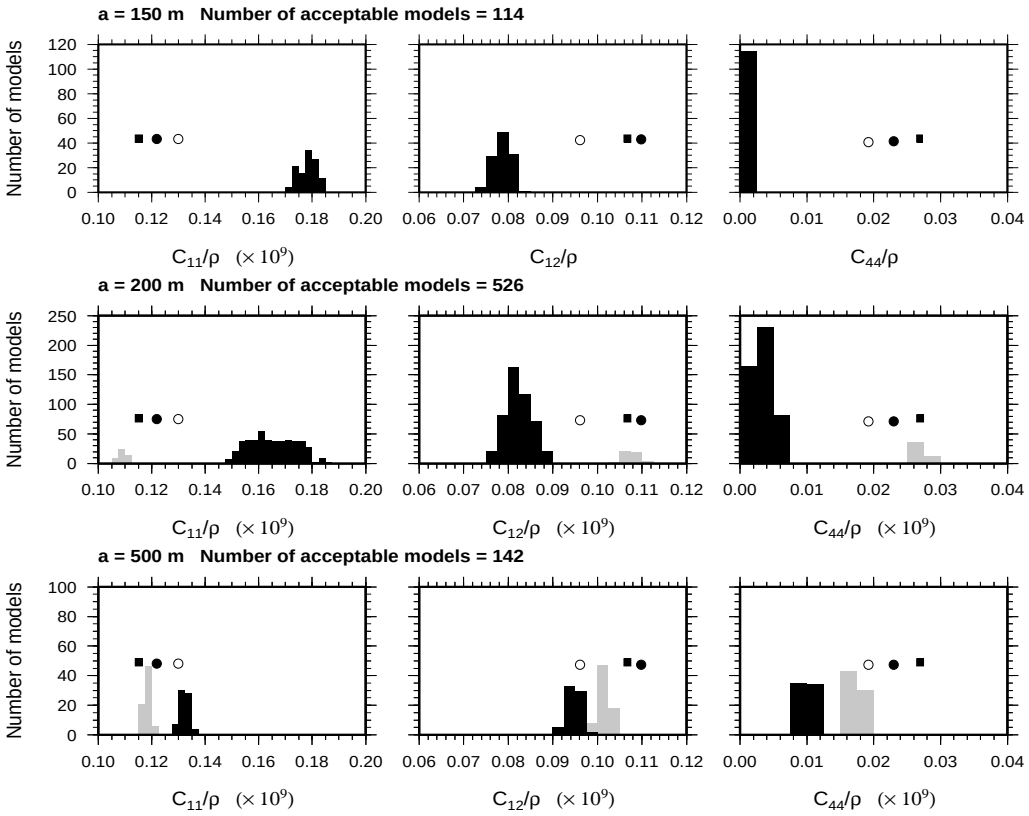

Fig. 8. Distribution of acceptable elastic constants C_{IJ}/ρ of cubic iron for different correlation lengths, indicated on top of each plot. At large correlation length, we observe two distinct families of cubic models (shown in grey and black). Circles correspond to two *bcc* iron models proposed by Vočadlo (2007) for a density $\rho = 13155$ kg.m^{-3} and a temperature T=5500 K (black), and for $\rho = 13842$ kg.m^{-3} and T=6000 K (white). The square corresponds to the *bcc* iron model proposed by Belonoshko et al. (2007) for a density $\rho = 13580$ kg.m^{-3} and a temperature T=6000 K.

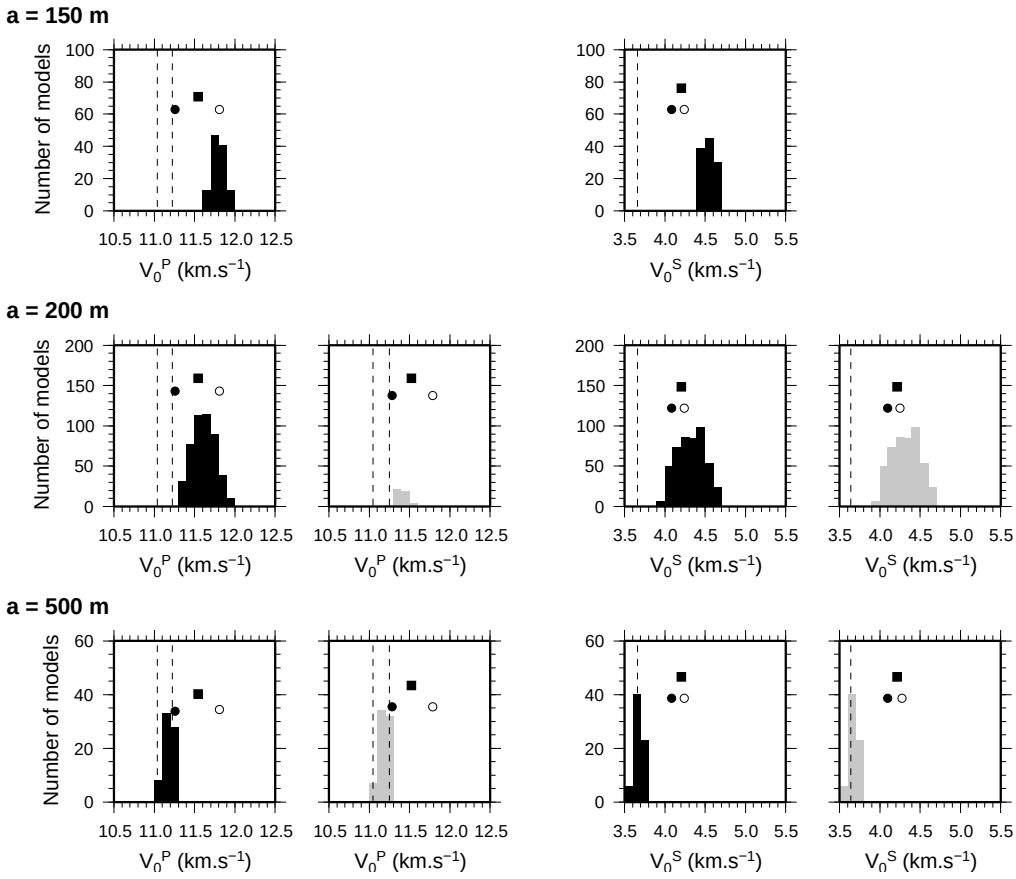

Fig. 9. Distribution of Voigt velocities for the two families of acceptable cubic models of iron shown in Figure 8. The correlation length is indicated on top of each plot: a =150, 200, 500 m. Circles correspond to the two *bcc* iron models proposed by Vočadlo (2007) and the square is the *bcc* model proposed by Belonoshko et al. (2007) (same symbols as in Figure 8). Vertical lines delimit the range of seismic velocities in the inner core.